Improving the diffuse optical imaging spatial resolution of the cerebral hemodynamic response to brain activation in humans

D. A. Boas, K. Chen, D. Grebert, and M. A. Franceschini

Anthinoula A. Martinos Center for Biomedical Imaging, Department of Radiology, Massachusetts General Hospital, Harvard Medical School, Charlestown, Massachusetts 02129

Received October 6, 2003

We compare two geometries of sources and detectors for optimizing the diffuse optical imaging resolution of brain activation in humans. Because of limitations in the instruments' dynamic range, most diffuse optical brain activation images have used only nonoverlapping measurements. We demonstrate theoretically and with a human experiment that a simple geometry of sources and detectors can provide overlapping measurements within the limitation of instrumentation dynamic range and produce an image resolution and localization accuracy that is twofold better. © 2004 Optical Society of America

OCIS codes: 170.5280, 170.6960, 170.3010.

The need within the neuroimaging community for portable and easy to use technologies for imaging brain function is motivating the further advancement of diffuse optical imaging methods. Diffuse optical methods were first used in 1993 to measure the hemodynamic response to brain activation.[1,2] Those first measurements used a maximum of five channels to distinguish brain activation in different brain regions. The first diffuse optical images of brain activation were published in 1995.[3] For the most part, all such images published to date were produced by analysis of the hemodynamic response measured with individual pairs of sources and detectors and then interpolation of the response between the measurement channels, as described in Refs. 3 and 4. These are essentially interpolation or backprojection procedures for producing images. The resolution is comparable to source–detector separation and quantitative accuracy is compromised because the image obtained is not an optimal solution of the inverse problem.[5] Here we refer to the image obtained by an optimal solution of the inverse problem as the diffuse optical tomography (DOT) image. There are only a few published examples of DOT images of brain hemodynamics, for example, in rodents,[6–9] in newborn human babies,[10] and in adult humans.[11] The advancement of true DOT for brain activation in humans would improve the image's spatial resolution and quantitative accuracy compared with those of current backprojection methods. Overlapping measurements are required for DOT to provide image quality that is significantly better than backprojection methods. However, the reflectance geometry used for measuring brain activation in humans requires a large detection dynamic range, particularly to support overlapping measurements in which a detector may be required to measure signals from nearby and far sources simultaneously. In this Letter we compare various geometries of sources and detectors for producing DOT images of brain activation from overlapping measurements. We then demonstrate, for the first time to our knowledge with an adult human brain activation experiment, the improvement in image resolution afforded by overlapping multidistance measurements.

We consider the two probe geometries shown in Fig. 1, i.e., a rectangular geometry of 9 sources and 16 detectors spanning 8.1 cm × 8.1 cm and a hexagonal geometry of 8 sources and 15 detectors spanning 9.8 cm × 8.5 cm. The rectangular geometry produces a large number (84) of measurements when nearest- and second-nearest-neighbor sources and detectors are considered but requires a large dynamic range, as the ratio of the longer source–detector separation to the shorter is 2.2. The hexagonal geometry reduces the dynamic range requirement, as the longer-to-shorter separation ratio is 1.7, but it produces only 50 measurements. We set the longer separation to 4.25 cm in each case, obtaining shorter separations of 1.9 and 2.5 for the rectangular and the hexagonal geometries, respectively. These shorter separations were chosen such that they would still have sensitivity (albeit weak) to the brain and the

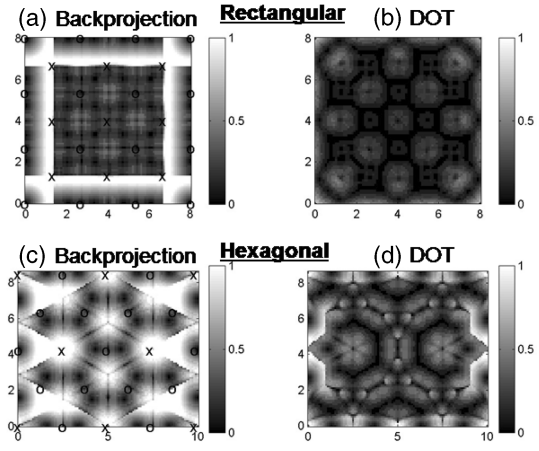

Fig. 1. Localization error for (a), (b) the rectangular and (c), (d) the hexagonal geometries compared for (a), (c) backprojection and (b), (d) DOT image reconstructions. The sources (crosses) and detectors (open circles) are shown in (a) and (c). The scale goes to 1 cm, where white indicates greater than 1-cm localization error.

0146-9592/04/131506-03$15.00/0

4.25-cm separation would still have a reasonable experimental signal-to-noise ratio (SNR). As we have measured on adult human subjects with our continuous-wave imaging system,[12] the signal decreases from shorter to longer separation are roughly 40 and 10 for the rectangular and hexagonal geometries, respectively. Maintaining a SNR of 100 thus requires dynamic ranges of at least 4000 and 1000, respectively. Given the strong optical attenuation in the adult human head and that we desire measurements with a bandwidth of a few hertz, our measurements must be made with sensitive photodetectors that generally do not have the required instantaneous dynamic range. Thus the effective dynamic range must be increased by time multiplexing of the sources and detector gains.[13] Turning each source on and off individually unnecessarily reduces the duty cycle and thus the SNR, assuming that instantaneous source power cannot be increased to maintain a constant average power. Frequency encoding strategies can be employed to multiplex different sets of sources (rather than individual sources) while optimal detectors gains are allowed for each source. This can be done with three sets of sources for the hexagonal geometry (sources 1, 5, and 6; 2 and 7; and 3, 4, and 8 in Fig. 2) but requires seven sets for the rectangular geometry. We do not consider the lattice geometry explored by Yamamoto *et al.*, [14] which is a variant of the rectangular geometry, as it is inferior to the geometries that we explored in the sense that it requires more sources and more detectors to produce fewer measurements.

For our simulations of imaging brain activation, we considered the probes shown in Fig. 1 placed on a homogeneous semi-infinite medium with $\mu_s' = 10\ \mathrm{cm}^{-1}$ and $\mu_a = 0.05\ \mathrm{cm}^{-1}$. The activation-induced localized increase in absorption occurred at depths of 1.5–2.0 cm. We utilized the linear Rytov approximation to the photon diffusion equation to identify changes in the measured photon fluence from spatial changes in the absorption coefficient.[5] That is, $\mathbf{y} = \mathbf{A}\mathbf{x}$, where the jth element of vector $\mathbf{x}$ indicates the absorption perturbation at the jth voxel and the ith element of the vector $\mathbf{y}$ represents the variation in the ith measurement that is due to spatial variation of absorption coefficient $\mathbf{x}$ from background absorption μ_a. Matrix $\mathbf{A}$ is the linearized transformation from image space $\mathbf{x}$ to measurement space $\mathbf{y}$. In our simulations we considered only a single image slice centered at a depth of 1.75 cm. Given a set of measurements $\mathbf{y}$, we calculated the DOT image, using Tikhonov regularization

$$\hat{\mathbf{x}} = \mathbf{A}^T(\mathbf{A}\mathbf{A}^T + \alpha s_{\max}\mathbf{I})^{-1}\mathbf{y}, \tag{1}$$

where $\mathbf{I}$ is the identity matrix, $s_{\max}$ is the maximum eigenvalue of $\mathbf{A}\mathbf{A}^T$, and α is the regularization parameter that we set to 10^{-3}. The singular value spectra of $\mathbf{A}\mathbf{A}^T$ for the two different source–detector geometries are similar, suggesting that the image information content of the two geometries is similar.[15,16] The rectangular geometry does have more image information that is provided by the additional measurements, but it is below the 10^{-3} noise level, such that practically speaking the two geometries have similar information content. We compared DOT image resolution with backprojection image resolution, where the backprojection image is given by[17]

$$\hat{\mathbf{x}} = (\mathbf{A}\mathbf{S})^T\mathbf{y}, \tag{2}$$

and diagonal matrix $\mathbf{S}$ produces column normalization (one-norm) of matrix $\mathbf{A}$.

For a quantitative comparison of the two geometries we calculated the image localization error and resolution. Image localization error and resolution can be determined from image resolution matrix $\mathbf{R}$, determined by substitution of $\mathbf{y} = \mathbf{A}\mathbf{x}$ into Eq. (1) such that

$$\mathbf{R} = \mathbf{A}^T(\mathbf{A}\mathbf{A}^T + \alpha s_{\max}\mathbf{I})^{-1}\mathbf{A}. \tag{3}$$

The same can be done with Eq. (2) to determine the resolution matrix for the backprojection image. The jth column of $\mathbf{R}$ reveals the image point-spread function for the jth voxel, from which we could determine image localization error and resolution. We calculated resolution w_j of an absorption perturbation in the jth voxel as the full area of the activation above the half-maximum of the peak activation

The localization error for the two geometries that use backprojection and DOT is shown in Fig. 1, whereas the resolution is shown in Fig. 3. These maps show how the localization error and the resolution vary for 1-mm^2 absorption increases that occur at different points across the image area. It is clear from Figs. 1 and 3 that the overlapping measurements utilized in the DOT image produce a significant improvement in the localization accuracy and resolution. The average localization errors over the image area for the rectangular geometry are 0.5 and 0.2 cm for the backprojection and the DOT images, respectively, a little better than the 0.7 and 0.3 cm found for the hexagonal geometry. The average resolutions over the image area for the rectangular geometry are 4.5 and 2.0 cm^2 for the backprojection and the DOT images, respectively, a little better than the 6.2 and 2.4 cm^2 for the hexagonal geometry.

To demonstrate experimentally the improved spatial resolution afforded by overlapping measurements, we utilized the hexagonal geometry because the reduced time sharing of sources increased our SNR relative

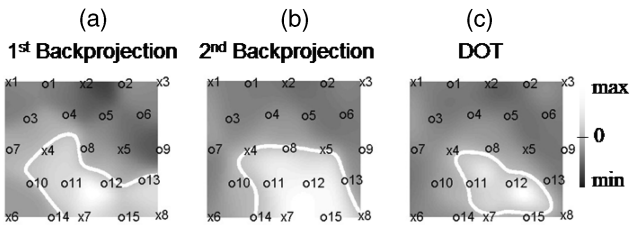

Fig. 2. Comparison of backprojection images obtained from first- and second-nearest-neighbor measurements with the DOT image. The positions of sources (crosses) and detectors (open circles) are indicated by the numbers in the reconstructed images. Solid curves, half-maximum contours.

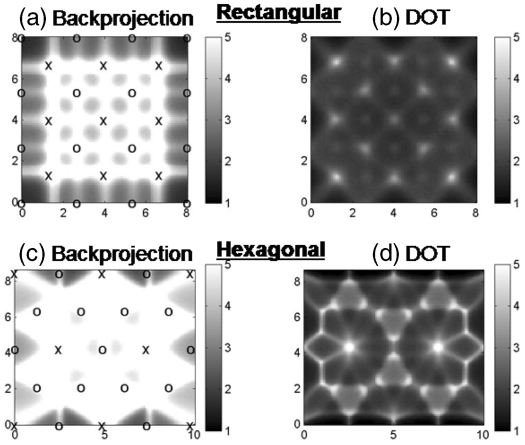

Fig. 3. Resolution for (a), (b) rectangular and (c), (d) hexagonal geometries compared for (a), (c) backprojection and (b), (d) DOT image reconstructions. The sources (crosses) and detectors (open circles) are shown in (a) and (c). The scale ranges from 1 to 5 cm^2, where white indicates greater than 5 cm^2.

to that of the rectangular geometry. We made measurements with our continuous-wave imaging system, which had 8 dual-wavelength source positions and 15 detectors.[12] Experiments were performed on healthy human adult volunteers as approved by Massachusetts General Hospital Institutional Review Board. The probes of sources and detectors were placed over the left motor cortexes of the volunteers, with the source–detector spacing as indicated in Fig. 1(c). One of the three subsets of sources was turned on and the detector gains optimized. Data were then collected for 600 s, with the subject alternating between tapping his or her fingers for 20 s and resting for 20 s for a total of 13 tapping cycles. The experiment was then repeated for each of the other two source sets with detector gains optimized accordingly. The raw experimental data were bandpass filtered from 0.016 to 1 Hz and block averaged; then DOT images were reconstructed from the 50 first- and second-nearest-neighbor measurements by use of Eq. (1) at a depth of 1.75 cm with $\mu_s' = 10\ cm^{-1}$ and $\mu_a = 0.05\ cm^{-1}$ and with regularization parameter $\alpha = 1$. The DOT image is compared in Fig. 2(c) with the backprojection images obtained by use of only the nearest- [Fig. 2(a)] or the second-nearest [Fig. 2(b)] neighbor measurements. Whereas we can see the increased absorption that is due to brain activation in the three different images in Fig. 2, the DOT image shows a smaller activation pattern of 18 cm^2 over the half-maximum activation value, compared with 30 and 32 cm^2 for the nearest and the second-nearest backprojection images. The DOT image resolution is clearly better. Whereas these values are all larger than that reported in the functional MRI literature, we note that the calculated area is strongly dependent on the image threshold that is used to determine activation, which is often set high in an fMRI experiment.

We have shown that incorporating second-nearest-neighbor measurements into a diffuse optical image reconstruction of brain activation significantly improves image resolution and localization accuracy by a factor of 2 compared with backprojection imaging with only nearest-neighbor measurements. We have compared rectangular and hexagonal geometries of sources and detectors and found that, whereas the rectangular geometry is slightly better, it is easier to implement the hexagonal geometry experimentally because the hexagonal geometry requires less switching between subsets of sources, has a greater measurement duty cycle, and requires a smaller dynamic range. We then experimentally demonstrated the significant improvement in image resolution afforded by a human brain function imaging experiment with the hexagonal geometry.

We thank Joe Culver for useful discussions of the analysis of image quality. We acknowledge financial support from National Institutes of Health grants P41-RR14075 and R01-EB002482. D. A. Boas's e-mail address is dboas@nmr.mgh.harvard.edu.

References

1. A. Villringer, J. Planck, C. Hock, L. Schleinkofer, and U. Dirnagl, Neurosci. Lett. **154,** 101 (1993).
2. Y. Hoshi and M. Tamura, Neurosci. Lett. **150,** 5 (1993).
3. A. Maki, Y. Yamashita, Y. Ito, E. Watanabe, Y. Mayanagi, and H. Koizumi, Med. Phys. **22,** 1997 (1995).
4. M. A. Franceschini, V. Toronov, M. Filiaci, E. Gratton, and S. Fantini, Opt. Express **6,** 49 (2000), http://www.opticsexpress.org.
5. S. R. Arridge, Inverse Probl. **15,** R41 (1999).
6. A. M. Siegel, J. J. A. Marota, and D. A. Boas, Opt. Express **4,** 287 (1999), http://www.opticsexpress.org.
7. A. M. Siegel, J. P. Culver, J. B. Mandeville, and D. A. Boas, Phys. Med. Biol. **48,** 1391 (2003).
8. J. P. Culver, T. Durduran, D. Furuya, C. Cheung, J. H. Greenberg, and A. G. Yodh, J. Cereb. Blood Flow Metab. **23,** 911 (2003).
9. J. P. Culver, A. M. Siegel, J. J. Stott, and D. A. Boas, Opt. Lett. **28,** 2061 (2003).
10. S. R. Hintz, D. A. Benaron, A. M. Siegel, A. Zourabian, D. K. Stevenson, and D. A. Boas, J. Perinat. Med. **29,** 335 (2001).
11. A. Bluestone, G. Abdoulaev, C. Schmitz, R. Barbour, and A. Hielscher, Opt. Express **9,** 272 (2001), http://www.opticsexpress.org.
12. M. A. Franceschini, S. Fantini, J. H. Thompson, J. P. Culver, and D. A. Boas, Psychophysiology **40,** 548 (2003).
13. C. H. Schmitz, H. L. Graber, H. Luo, I. Arif, J. Hira, Y. Pei, A. Bluestone, S. Zhong, R. Andronica, I. Soller, N. Ramirez, S. Barbour, and R. L. Barbour, Appl. Opt. **39,** 6466 (2000).
14. T. Yamamoto, A. Maki, T. Kadoya, Y. Tanikawa, Y. Yamada, E. Okada, and H. Koizumi, Phys. Med. Biol. **47,** 3429 (2002).
15. J. P. Culver, V. Ntziachristos, M. J. Holboke, and A. G. Yodh, Opt. Lett. **26,** 701 (2001).
16. H. Xu, H. Dehghani, B. W. Pogue, R. Springett, K. D. Paulsen, and J. F. Dunn, J. Biomed. Opt. **8,** 102 (2003).
17. S. A. Walker, S. Fantini, and E. Gratton, Appl. Opt. **36,** 170 (1997).